The tensile properties of a Powder Metallurgy Cu-Mo-Ni diffusion bonded steel sintered at different temperatures

D. Toledo Dos Santos[1], A. Salemi[2], I. Cristofolini[1], A. Molinari[1]

[1] University of Trento, Trento (Italy)

[2] Sinteris SpA, Bentivoglio, Bologna (Italy)

Abstract

The increase of the sintering temperature from 1120°C up to 1280°C of a 0.2%C Cu-Mo-Ni diffusion bonded steels with 6.9 g/cm^3 and 7.2 g/cm^3 green density slightly increases sintered density and improves the pore morphology. The fraction of the load bearing section increases consequently. Moreover, high sintering temperature enhances the compositional homogeneity of the metallic matrix, and the microstructure evolves from a mixture of ferrite, pearlite, bainite, martensite and Ni-austenite to a bainitic/martensitic microstructure, with a decreasing amount of the Ni-austenite. Tensile strength and ductility increase with the sintering temperature. The paper clearly demonstrates the role of the pore morphology on the mechanical properties that are therefore better correlated to the fraction of the load bearing section than to density. It also highlights that sintering temperature may represent a solution to enhance mechanical properties of porous sintered steels as an alternative to the increase in green density.

Keywords: sintering temperature; fraction of load bearing section; tensile strength; tensile ductility

1. Introduction

The positive effect of a high sintering temperature on mechanical properties of Powder Metallurgy (PM) steels is recognized since years [1, 2]. However, in the industrial practice the carbon and low alloy Ni, Mo, Cu alloyed steels are sintered in continuous belt furnaces at temperatures between 1100°C and 1180°C, since the resulting mechanical properties are high enough to match the technical requirements of many structural parts used in different applications and, in particular, in the automotive industry. Sintering at temperature above 1180-1200°C cannot be carried out in belt furnaces, mostly because of the too rapid damage of the belts. The more expensive roll and walking beam continuous furnaces or batch furnaces must be used, that results in an unacceptable increase of the production costs, vanishing the cost effectiveness of PM in comparison to alternative technologies. Due to these technical and economical reasons, sintering temperature is defined as high when it exceeds 1180-1200°C.

In sintering of chromium alloyed steels, the sintering temperature should be raised at 1240°C and above, to effectively reduce the highly stable chromium oxide on the surface of the powder particles, thanks to the carbothermal reduction mechanism [3]. The high sintering temperature has an additional advantage resulting from the enhancement of the mass transport phenomena responsible for the neck growth, that results in an increased densification and in the improvement of the pore morphology [4]. Such an advantage may be

exploited in Cr-free sintered steels, as shown by Stoyanova et al. in their work on the impact strength of Mo and Ni low alloyed steels [5].

The increase in sintering temperature enhances densification and neck growth and improves the morphology of the residual pores, that display an increasingly rounding of edges when temperature is raised. Chawla and Deng demonstrated that tensile and fatigue strength increase with density and pore rounding [6], therefore the increase in the mechanical properties with sintering temperature may be attributed both to the enhanced densification and to the improved pore morphology.

The mechanical properties of porous sintered materials may be successfully correlated to the fraction of the load bearing section Φ and to the mechanical properties of the metallic matrix. Simple relations were proposed by Ashby and Gibson for the Young's modulus [7], by Straffelini et al. for the tensile strength [8], by Cope et al. for tensile ductility [9], by Molinari et al. [10] for the impact strength. All these relations will be used in the following.

Φ can be determined from porosity and the pore morphology [10] and increases with the sintering temperature [11]. The mechanical properties of the metallic matrix depend on its microstructure. A very peculiar case in Powder Metallurgy (PM) is represented by the steels produced with diffusion bonded powders. The alloying elements (mostly Ni and Cu) are added as fine particles bonded to the coarser iron particles by partial diffusion, to prevent the risk of segregation during transportation and handling, maintaining the excellent compressibility of pure iron. Since the solid state diffusivity of Cu, Ni and Fe at the sintering temperature is not high enough to achieve a homogeneous distribution of alloying elements, the as-sintered microstructure may comprise all the possible products of the transformation of austenite on cooling and some untransformed Ni-rich austenite. The influence of the processing parameters on such an inhomogeneous microstructure has been investigated by Castro et al. [12] and by Sainz et al. [13] who demonstrated that the compositional and microstructural heterogeneity cannot be completely removed. The mechanical properties of these materials have been deeply investigated by several authors, with particular attention on the effect of the soft and ductile Ni-austenite on fatigue behaviour. Deng et al. observed that the crack growth in Ni-rich regions is up to three times as fast as through coarse pearlite [14]. On the contrary, Carabajar et al. concluded that the Ni-rich austenite may delay or prevent the nucleation and propagation of cracks both under monotonic and cyclic loading [15, 16]. Abdoos confirmed these results observing crack arrest or circumvention in the Ni areas [17]. Recently, Gilmas demonstrated that sintered steels containing the Ni-austenite may reach a higher damage before fracture, due to its ductility [18]. Same result was reported by Sori et al. [19]. On the contrary, Bennier et al. did not found an effect of Ni-austenite on fatigue resistance [20]. The Ni-austenite enhances the impact strength [5] thanks to its ductility and the stress induced martensitic transformation [21]. The low hardness of Ni-austenite affects the wear resistance negatively, as demonstrated by Metinoz et al. [22].

Sainz et al. [13] have demonstrated that even when sintered at high temperature the steels produced with admixed Ni (they are very similar to those obtained with diffusion bonded powders) have a heterogeneous microstructure, with a decreasing amount of the Ni-austenite on increasing temperature. The effect of the

sintering temperature on the mechanical properties is the result of the combination of the improved fraction of the load bearing section and of the decrease of the content of the soft and ductile Ni-austenite. While yield strength is expected to increase, the influence on tensile elongation and, in turn, on tensile strength is doubtful.

In the present paper, the tensile properties of a low carbon 4%Ni, 2%Cu and 0.5%Mo obtained with a diffusion bonded powder and sintered at 1120°C, 1230°C and 1280°C are investigated. The specimens were compacted to two different green densities to compare the effect of the increase in the sintering temperature to that of green density in the typical density range of the structural components produced by PM industry.

2. Materials and Methods

The material of this study is a steel obtained by mixing the diffusion bonded Cu-Ni-Mo iron powder (4%Ni, 1.5%Cu, 0.5%Mo nominal composition), with 0.2% graphite and 0.6% lubricant. Tensile specimens were produced in accordance with the ISO 2740. They were compacted to 6.9 and 7.2 g/cm^3 (green density) and sintered:

- at 1120°C with 30 minutes isothermal holding in a belt furnace and
- at 1230°C and 1280°C, 40 minutes isothermal holding, in a vacuum furnace with nitrogen backfilling at 900°C.

Density of the specimens was measured with the Archimedes' principle (ASTM B962 – 17). Pore morphology was investigated by quantitative metallography using the Light Optical Microscope (LOM). Five images of non-etched specimens were taken at 200× magnification from the metallographic cross section using a Leica QWin Standard V. 2.5 software. Pore parameters D_{circle}, f_{circle} and f_{shape} were calculated for each pore detected. D_{circle} is the diameter of a circle with the same area as the cross-section of the pore investigated and is representative of the pore size. f_{shape} and f_{circle} represent the roundness and the smoothness of the profile of the pores, respectively; they are defined by equations (1) and (2):

$$f_{shape} = \frac{D_{min}}{D_{max}} \quad (1)$$

Where D_{mm} and D_{max} represent the minimum and the maximum Feret diameter, respectively.

$$f_{circle} = \frac{4.\pi.A}{P^2} \quad (2)$$

Where A and P represent the area and the perimeter of the pore.

The values of these parameters range from 0 to 1, where 1 means a circular shape with smooth profile and values close to 0 represent pores with a very elongated shape and a highly rugged profile.

The metallographic specimens were etched using Nital 2%, and microstructure was investigated at the LOM. The distribution of the alloying elements was investigated by EDXS at the Scanning Electron Microscope (SEM).

The content of Ni-austenite was measured by X-Ray Diffraction (XRD), using the CrKα radiation.

HV 0.1 microhardness was measured on the metallographic sections. Tensile tests (ASTM E8/E8M) were performed with an Instron testing machine using a 12 mm extensometer to measure elongation. The strain speed was 1 mm/min.

3. Results

Sintered density and porosity of specimens are shown in Figures 1 and 2, respectively, as a function of the sintering temperature.

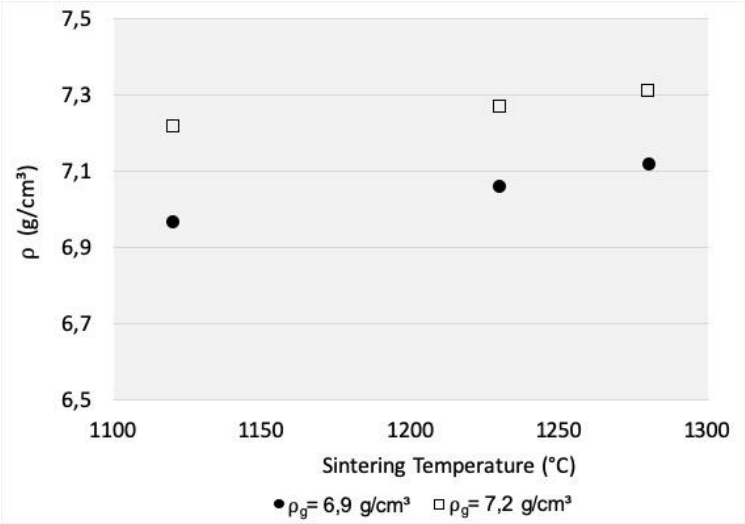

Figure 1 – The effect of green density and sintering temperature on sintered density.

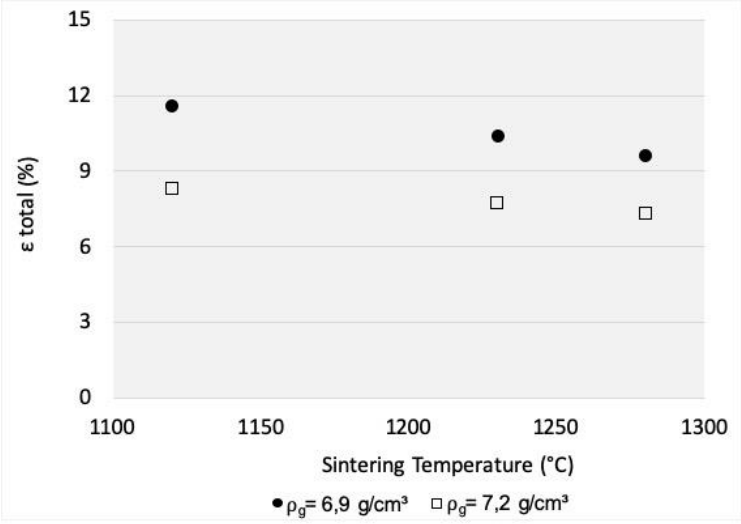

Figure 2 – The effect of green density and sintering temperature on the total porosity.

Density slightly increases with the sintering temperature and porosity decreases accordingly. It's worthy to observe that the specimens with ρ_{green}= 6.9 g/cm³ even when sintered at 1280°C present a lower density than those with ρ_{green}= 7.2 g/cm³ sintered at 1120°C, meaning that the increased densification promoted by temperature does not compensate for the lower green density.

The porosity of the sintered specimens is shown in the micrographs of figure 3.

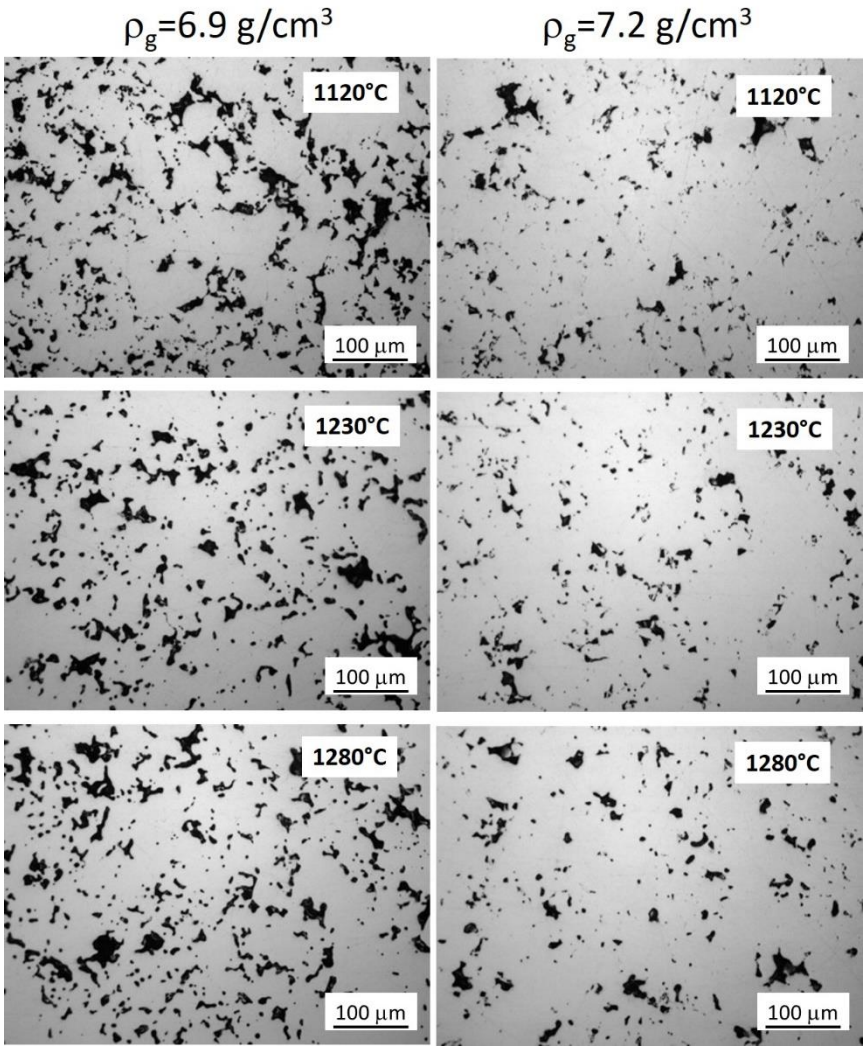

Figure 3 – LOM images of specimens sintered at different temperatures.

The images display a progressive rounding of the pore edges with increasing the sintering temperature. The comparison between the distributions of frequency and the cumulative curves of f_{circle}, f_{shape} and D_{circle} is presented in figure 4a, 4b and 4c, respectively.

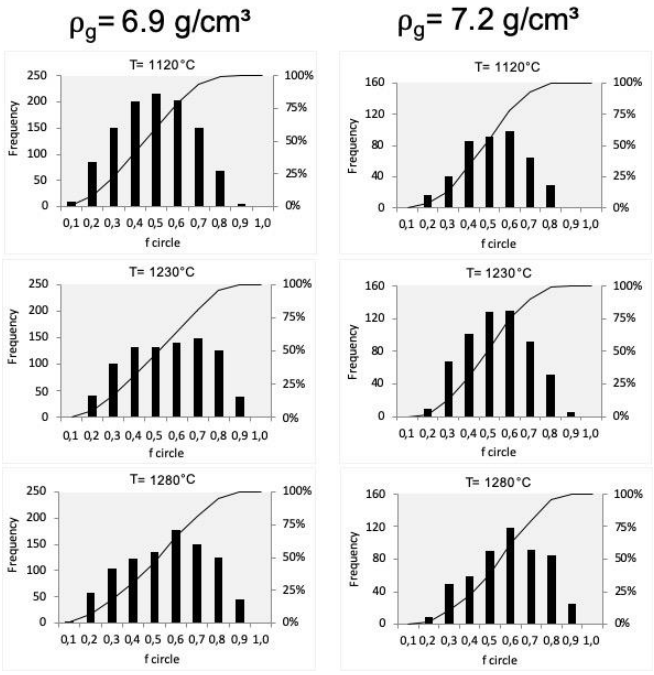

Figure 4a – Frequency distributions and cumulative curves of f_{circle} for specimens with different sintered at different temperatures.

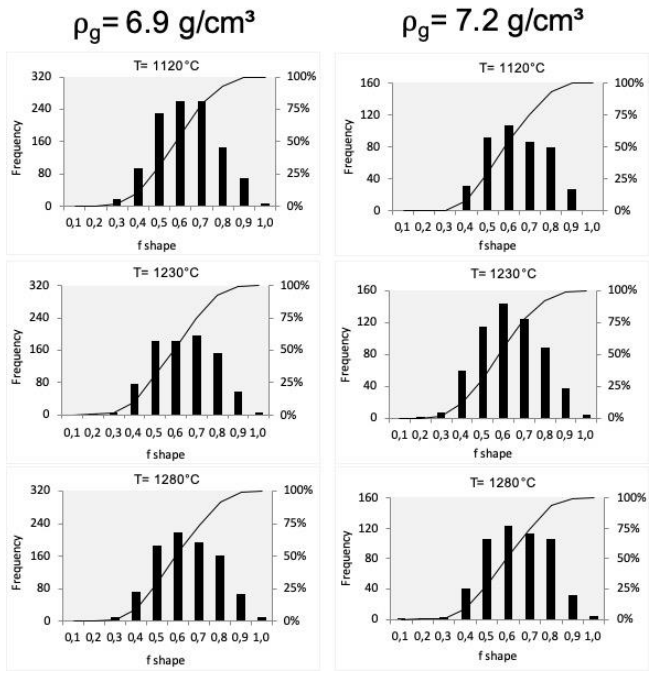

Figure 4b – Frequency distributions and cumulative curves of f_{shape} for specimens with different sintered at different temperatures

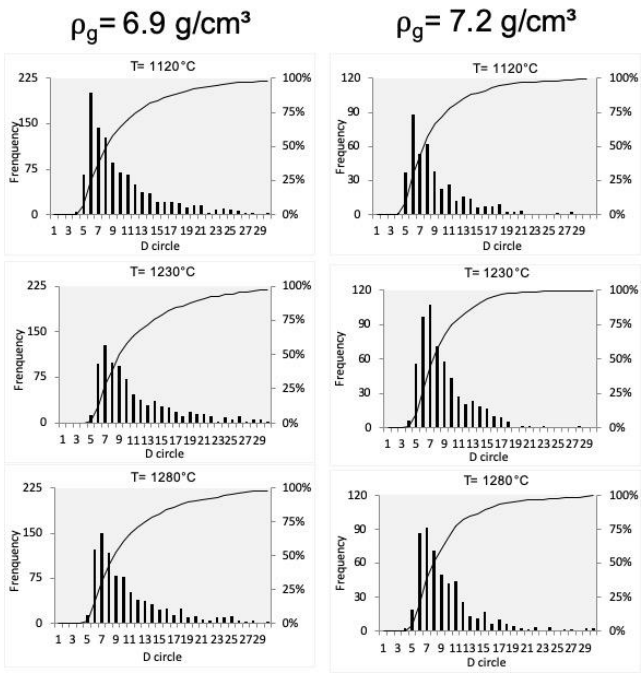

Figure 4c – Frequency distributions and cumulative curves of D_{circle} for specimens with different sintered at different temperatures

The f_{circle} and f_{shape} distributions shift toward 1 with increasing sintering temperature, confirming the improvement of the pore morphology observed in figure 3. This trend is observed on materials with both green densities. D_{circle} distribution shows that pore size is smaller for the specimens with higher green density, while sintering temperature does not display any evident effect.

Figure 5 shows the etched microstructure of the materials.

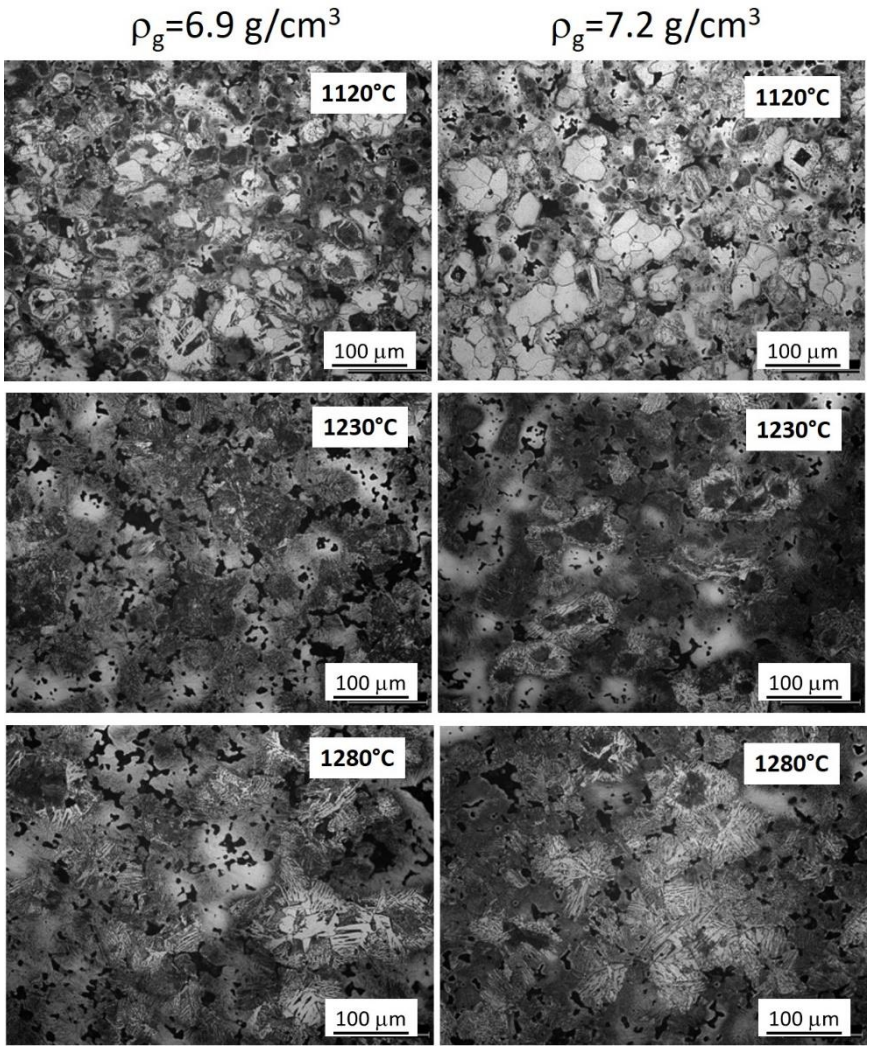

Figure 5 – LOM microstructure of specimens sintered at different temperatures and etched with 2% Nital

Specimens sintered at 1120°C display the well-known inhomogeneous microstructure of diffusion alloyed materials where martensite, pearlite, bainite, Ni-rich austenite and ferrite can be observed. The specimens sintered at 1230°C present bainite, martensite with some pearlite nodules and a few small regions of Ni-rich austenite; ferrite is absent. At 1280°C, the microstructure displays more bainite and less martensite than at 1230°C, no pearlite and still a few regions of Ni austenite. The microstructural evolution is due to the improved compositional homogenization of the material promoted by the increase in the sintering temperature. Figure 6, 7 and 8 show the SEM microstructure and the EDXS maps of Ni, Mo and Cu of the three materials with 6.9 g/cm^3 green density sintered at the three temperatures. They are representative of the specimens with the higher green density.

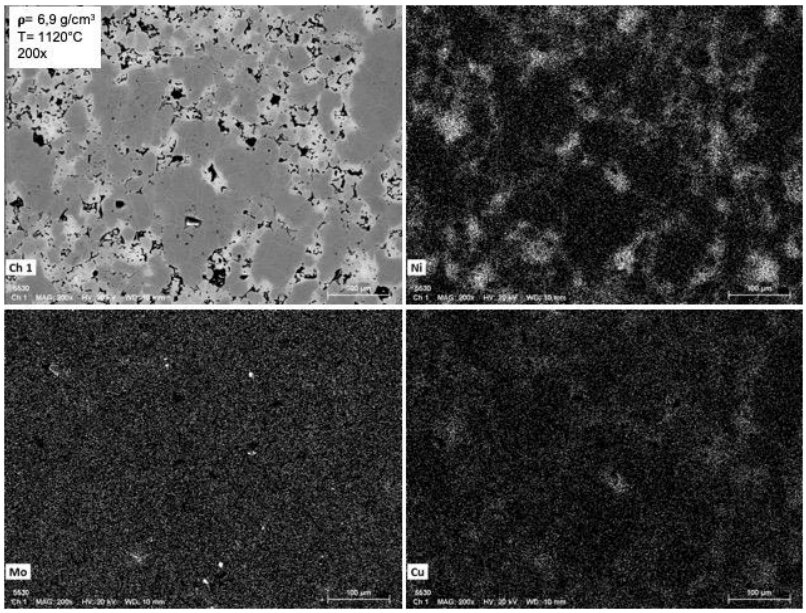

Figure 6. SEM microstructure and Ni, Mo and Cu EDXS maps of the materials with 6.9 g/cm^3 green density sintered at 1120°C

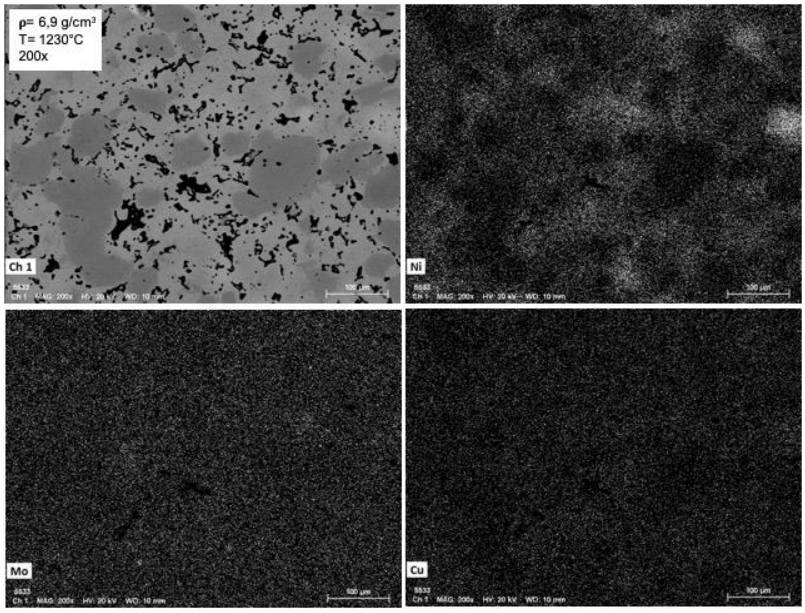

Figure 7. SEM microstructure and Ni, Mo and Cu EDXS maps of the materials with 6.9 g/cm^3 green density sintered at 1230°C

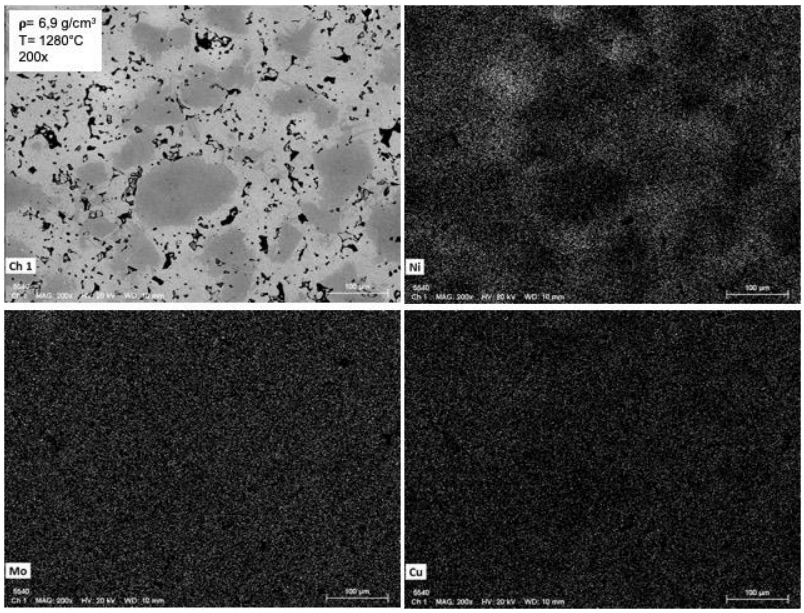

Figure 8. SEM microstructure and Ni, Mo and Cu EDXS maps of the materials with 6.9 g/cm^3 green density sintered at 1280°C

At 1120°C, Ni and Cu are segregated around the ferrous particles while Mo is homogenously distributed. With increasing temperature Cu displays an almost homogeneous distribution, while Ni is still segregated, even if less than at 1120°C. The Ni concentration in the segregated areas is much less at 1230°C than at 1120°C, and even slightly less at 1280°C. The amount of the Ni stabilized austenite decreases consequently, as confirmed by XRD analyses that result in 8±2%, 3±2% and 2±2% in specimens sintered at 1120°C, 1230°C and 1280°C, respectively, with no significant differences due to green density.

Microhardness was used by Mingard and Roebuck to map the microstructure of diffusion bonded sintered steels [23]. They used a Scanning Indentation Microhardness Machine (SIMM) to obtain hundreds of micro-indentations, from the distribution of which they could identify the microstructural constituents. In the present work, a different approach was used, by realizing a few tens of random indentations using a standard microhardness tester. Table 1 reports the results of HV0.1 measurements on the six materials; the minimum and maximum values along with the median are reported.

Table 1. Microhardness of the materials investigated

Sintering temperature	Green density	$HV0.1_{min}$	$HV0.1_{max}$	$HV0.1_{50}$
1120°C	6.9 g/cm^3	129	201	160
	7.2 g/cm^3	106	182	140
1230°C	6.9 g/cm^3	184	632	310
	7.2 g/cm^3	157	406	300
1280°C	6.9 g/cm^3	186	468	186
	7.2 g/cm^3	175	318	175

With increasing temperature, the median and the maximum microhardness are the lowest at 1120°C and the highest at 1230°C. Moreover, microhardness is basically higher in the specimens with the lowest green density. These results are coherent with the microstructural analysis, that displays a larger amount of martensite in the specimens sintered at 1230°C than at 1280°C, and the absence of ferrite and pearlite and a less amount of Ni austenite at both temperatures than at 1120°C, as well as a greater amount of martensite in the low density specimens.

In figure 9 and 10, examples of stress-strain tensile curves for each sintering temperature are presented for specimens with ρ_{green} = 6.9 g/cm³ and 7.2 g/cm³, respectively.

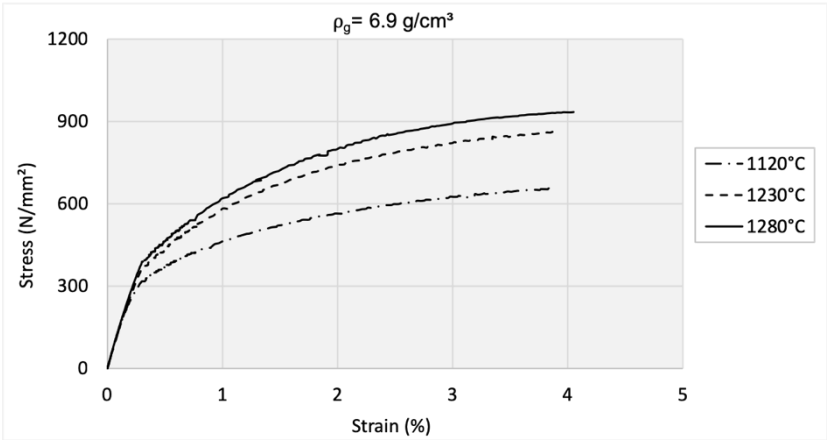

Figure 9 – Tensile curves for each sintering temperature for specimens with ρ_g = 6.9g/cm³.

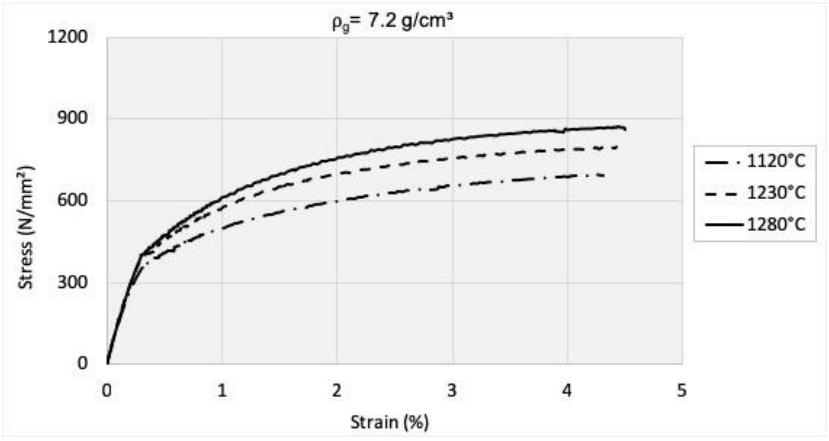

Figure 10 – Tensile curves for each sintering temperature for specimens with ρ_g = 7.2g/cm³.

The graphs show that stress and strain increase with the sintering temperature. Table 2 reports Young's modulus (E), yield strength (σ_y), Ultimate Tensile Strength (UTS) and elongation at fracture (ε) of all the materials.

Tab. 2: mechanical properties of the investigated materials

Green density	Sintering temperature	E (GPa)	$\sigma_{y0.2}$ (MPa)	UTS (MPa)	ε (%)
6.9 g/cm^3	1120 °C	142	341	606	3.7
	1220 °C	143	426	847	4.0
	1280 °C	152	478	894	4.0
7.2 g/cm^3	1120 °C	153	401	668	4.3
	1220 °C	155	456	819	4.5
	1280 °C	159	481	876	4.5

All the properties determined form the tensile tests increase increasing the green density and with the sintering temperature.

4. Discussion

Sintering temperature affects the pore morphology. Its effect is more pronounced on f_{circle} than on f_{shape}, as it was observed in previous works [24]. This result may be justified considering the physical meaning of the two parameters. As mentioned in the previous section f_{circle} is representative of the smoothness of the pore profile while f_{shape} represents the pore roundness. As shown in figure 11, the improvement of the former requires a less intense mass transport over a smaller diffusion distance than the improvement of the latter; therefore, the improvement of pore profile is achieved faster than that of the pore roundness.

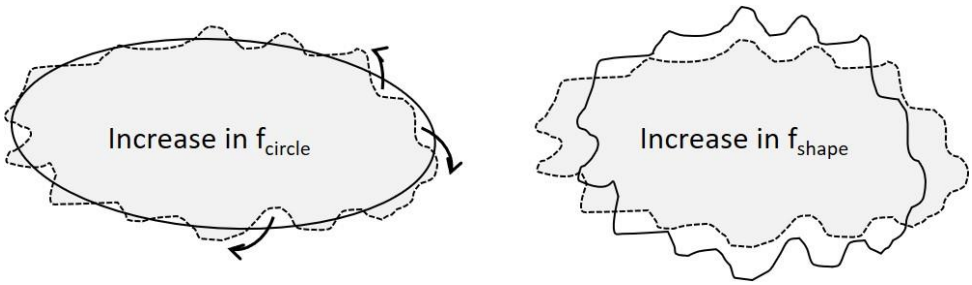

Fig. 11 – Schematic representation of mass transport phenomena responsible for the increase in f_{circle} and in f_{shape}: dotted line for pore in the green state, continuous line for pore in the sintered state

As far as the microstructure of the matrix is concerned, at 1120°C, Ni and Cu are segregated. With the increasing temperature, Cu reaches an almost homogeneous distribution, while Ni is less segregated than at 1120°C, due to the enhanced iron diffusion into the Ni-rich areas [11, 12] promoted by the increase in temperature.

The metallographic analysis (Figure 5) indicates a greater content of martensite in the lowest density specimens at the same sintering temperature. The cooling rate from the sintering temperature is not affected by porosity, as reported by Saritas who measured the actual temperature of Jominy bars with different density [25]. In

liquid phase sintering, the increase in the green density opposes the spreading of the liquid copper among the solid particles [26]. Copper may therefore result more homogeneously distributed in the low density specimens, and thanks to its effect on hardenability it may favor the formation of a greater amount of martensite on cooling from the sintering temperature.

The increase in the content of hard microstructural constituents achieved by increasing temperature does not cause a decrease of tensile elongation (Table 2), due to the slight increase in the sintered density and to the improvement in the pore morphology. In spite of the embrittlement of the metallic matrix caused by the microstructural evolution with temperature, the increase in the fraction of the load bearing section ensures an increment of ductility.

The fraction of the load bearing section was determined with eq. (3) [10],

$$\Phi = [1 - (5.58 - 5.57 \times f_{circle})\varepsilon]^2 \quad (3)$$

Where f_{circle} is the median value and ε is the fractional porosity acquired by image analysis.

Figure 12 shows the fraction of load bearing section calculated for each sintering temperature and green density.

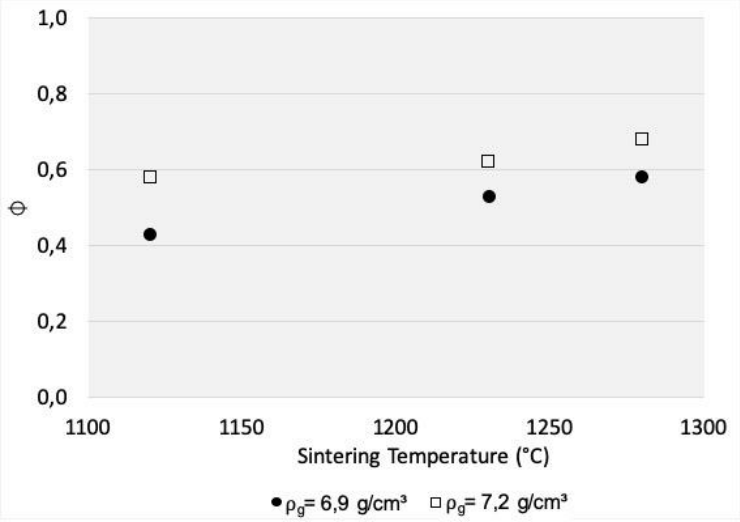

Figure 12 – Influence of green density and sintering temperature on the fraction of the load bearing section.

The figure highlights the noticeable effect of the sintering temperature; in spite of the slight densification (fig. 1), the fraction of the load bearing section increases noticeably with the sintering temperature due to the improvement of the pore morphology. Sintering at 1280°C of the lowest green density specimens leads to the same fraction of the load bearing section achieved by sintering at 1120°C the specimens compacted to 7.2 g/cm^3. Differently from what observed with density, in case of the fraction of the load bearing section increasing the sintering temperature can compensate for the lower green density.

In Figure 13 Young's modulus, yield strength, tensile strength and elongation at fracture are plotted vs Φ.

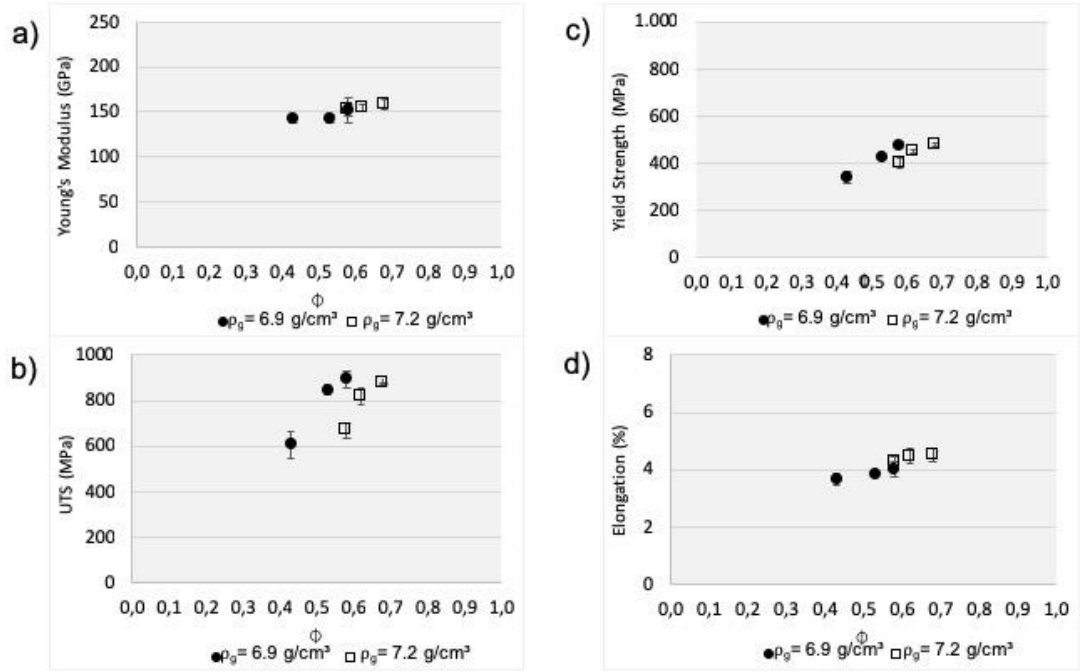

Figure 13 – Mechanical properties vs. the fraction of load bearing section: a) Young's Modulus, b) UTS, c) Yield Strength and d) Elongation.

The Young's modulus and elongation at fracture present a unique correlation with the fraction of load bearing section for the six material, whilst yield strength and ultimate tensile strength depict two distinct correlations for each green density. This is due to the effect of green density on the mechanical properties of the metallic matrix, that may be deduced from the microstructure and the microhardness. Yield strength and UTS are correlated to Φ by equations (4) and (5) [8]

$$\sigma_y = \sigma_{y0}\Phi \qquad (4)$$

$$UTS = UTS_0\Phi \qquad (5)$$

where σ_{y0} and UTS_0 are the properties of the metallic matrix (of the pore free materials). Both yield and tensile strength of the matrix of the 6.9 g/cm^3 specimens are expected to be higher than those of the 7.2 g/cm^3 specimens, due to the higher microhardness. Therefore, at the same fraction of the load bearing section yield strength and Ultimate Tensile Strength of the lower density material are higher than those of the high density ones. Since elastic modulus of steel is almost independent on its microstructure, E of the metallic matrix is independent on green density. Figure 14 shows that all the six materials match the Ashby model for the elastic modulus [7]

$$E = E_0\sqrt{\Phi} \qquad (6)$$

Where E_0 is the Young's modulus of the matrix. Finally, tensile elongation is correlated to Φ by the Cope model

$$\varepsilon = \varepsilon_0 \Phi^{\frac{3}{2}} \qquad (7)$$

Where ε_0 is the tensile elongation of the matrix. In principle, ε_0 should depend on green density, due to the different microstructure of the matrix. But, since in the neck regions, where localized deformation occurs determining the ductility of the porous material, the microstructure is almost martensitic in all the specimens [12, 13], tensile elongation of the matrix is not affected by green density, and the experimental points in figure 14 depict one single correlation.

In order to evaluate the effect of the increase in the sintering temperature on the mechanical properties, in figure 14 the increments of Young's modulus, yield strength, UTS and elongation at fracture achieved by sintering at high temperature are reported. The reference is the material compacted to 6.9 g/cm^3 and sintered at 1120°C.

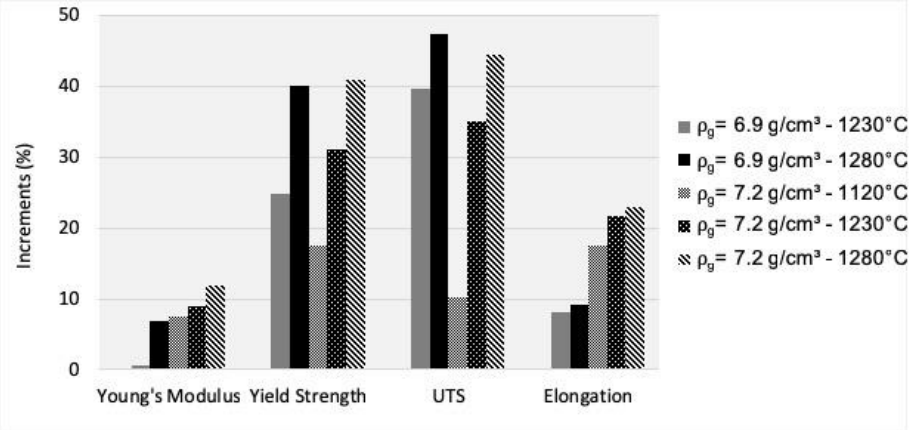

Figure 14 – Increments over sintering at 1120°C with ρ_{green}= 6.9g/cm³.

The properties that are more significantly increased by sintering temperature are yield and tensile strength. These properties increase by 30-40% with reference to the low density material sintered at 1120°C, independently on the green density. The increase in tensile elongation is lower and depends on green density. The different effect of the sintering temperature on strength and ductility derives from the evolution of the matrix since on increasing temperature the metallic matrix becomes harder, i.e. more resistant and less ductile. The increase in strength is synergic with the increase in the fraction of the load bearing section, the decrease of ductility attenuates the effect of the increase in Φ. The effect on Yong's modulus is rather small and slightly affected by green density.

5. Conclusion

The effect of the sintering temperature on density, pore morphology and microstructure and its effect on the tensile properties of a 0.2%C Cu-Mo-Ni diffusion bonded steels with two different green densities was studied. With increasing the sintering temperature from 1120°C up to 1280°C, sintered density slightly increases, pore morphology gets better, in particular the irregularity of the pore profile, whilst the pore size does not change significantly. Mechanical properties depend on density and on the pore morphology; these two characteristics may be combined in the definition of the fraction of the load bearing section that is the cross section of the specimen effectively bearing the load. Starting from a 6.9 g/cm^3 green density and a sintering temperature of 1120 °C, that represent usual processing conditions in the industrial practice, the fraction of the load bearing section display the same increment either on compacting to 7.2 g/cm^3 or by sintering at 1280°C. In the former case, it increases due to the increased density, in the latter due to the improved pore morphology.

Mechanical properties depend also on the microstructure of the metallic matrix. The increase in the sintering temperature improves the compositional homogeneity of the matrix but the fully homogenization is not achieved. The microstructure evolves from a mixture of ferrite, pearlite, bainite, martensite and Ni-austenite to a bainitic/martensitic microstructure, with a decreasing amount of the Ni-austenite. Due to the evolution of the distribution of the alloying elements, the amount of martensite increases from 1120°C to 1230°C and decreases at 1280°C. The microhardness of the metallic matrix changes coherently with the evolution of the microstructure, presenting the highest values at 1230°C.

Tensile properties were then correlated to the fraction of the load bearing section and to the microstructure of the matrix, to interpret the effect of sintering temperature. Tensile strength increases with the sintering temperature due to the microstructural strengthening and the increased fraction of the load bearing section. No effect of green density is observed on the tensile strength when sintering is carried out at 1230°C and at 1280°C. In spite of the microstructural strengthening promoted by the increase in the sintering temperature, tensile ductility increases due to the improved fraction of the load bearing section. In this case, there is an effect of the green density that compensates for the effect of the decreased ductility of the matrix when temperature is increased.

The paper demonstrates that mechanical properties of porous sintered steels cannot be simply correlated to density, since the important effect of the pore morphology is neglected. From a technological viewpoint sintering temperature may represent a solution to enhance mechanical properties of porous sintered steels as an alternative to the increase in green density, in particular in parts whose geometrical complexity makes it difficult the achievement of green density above 7.0 g/cm^3.

Data Availability statement. The raw/processed data required to reproduce these findings cannot be shared at this time as the data also forms part of an ongoing study.

References

1. U. Engstrom, Adv. Powd. Metall. Part. Mater. 2(7)(1999)86
2. A. Pietrovski, G. Biallas, Powd. Metall. 41(2)(1998)109
3. H. Danninger, R. de Oro Calderom, C. Gierl-Mayer, Chemical reactions during sintering of PM steel compacts as a function of the alloying route, Powd. Metall. 61(3)(2018)241-250
4. V. Stoyanova, A. Molinari, Powd. Metall. Progr. 3(2)(2003)86
5. V. Stoyanova, A. Molinari, Vacuum sintering and sinter-hardening of Mo and Ni low alloyed steels, Powder Metallurgy Progress 4(2)(2004)79
6. N. Chawla, X. Deng, Microstructure and mechanical behavior of porous sintered steels, Mater. Sc. Eng. A 390 (2005) 98–112
7. M.F. Ashby, L.J. Gibson, "Cellular Solids" Pergamon Press, 1988
8. G. Straffelini et al., Powder Metallurgy 45(2)(2002)167
9. L. Cope, Metallurgia, 72(1965)165
10. A. Molinari, C. Menapace, E. Santuliana, G. Straffelini, A simplified model for the impact resistance of porous sintered steels, Powd. Metall. Progr. 11(1-2)(2011)12-20
11. I. Cristofolini, A. Molinari, S. Tesfaye, M. Federici, A. De Nicolò, H. Weber, High temperature sintering: microstructure, density, dimensional and geometrical precision, Advances in Powder Metallurgy and Particulate Materials 5(2014)213-221
12. F. Castro, A, Veiga, S. Sainz, A. Karuppanagounder, D. Jorge, Influence of sintering cycle and chemical composition on the amount of martensite obtained after cooling of PM nickel steels, Proceedings EuroPM2013, Gothenburg (Sweden) 15-18 September 2013,
13. S. Sainz, W. Garcia, A. Karuppanagounder, F. Castro, Microstructural development during sintering of PM steels with admixed nickel, Powder Metall. Prog. 7(2017)121-127
14. X. Deng, G. Piotrowski, N. Chawla, K.S. Narasimhan, Fatigue crack growth behavior of hybrid and prealloyed sintered steels Part II. Fatigue behaviour, Mater. Sc. Eng. A 491 (2008) 28–38
15. S. Carabajar, C. Verdu, R. Fougeres, Damage mechanisms of a nickel alloyed sintered steel during tensile tests, Mater. Sc. Eng. A 232 (1997)80-87
16. S. Carabajar, C. Verdu, A. Hamel, R. Fougeres, Fatigue behaviour of a nickel alloyed sintered steel, Mater. Sc. Eng. A 257 (1998)225-234
17. H. Abdoos, H. Khorsand, A.R. Shahani, Mater. Des. 30(2009)1026-1031
18. M. Gilmas, J. Chottin, M.J. Dougan, E. Hug, Evolution of damage and fracture in two families of Ni-Cu-Mo sinter-hardened steels with various initial porosities, Mater. Sc. Eng. A 654(2016)85-93
19. M. Sori, T. Vuehrer, S. Glodez, Fatigue and fracture parameters of diffusion alloyed Cu-Ni-Mo sintered steels, Eng. Fract. Mech. 153(2016)278-288
20. F Bernier, P Plamondon, J.P Baïlon, G L'Espérance, Microstructural characterisation of nickel rich areas and their influence on endurance limit of sintered steel, Powd. Metall. 54(2011)559-565

21. M.W. Wu, L.C. Tsao, G.J. Shu, B.H. Lina, The effects of alloying elements and microstructure on the impact toughness of powder metal steels, Mater. Sc. Eng. A538(2012)135-144

22. I. Metinoz, I. Cristofolini, A. Molinari, Influence of Ni Content on Dry Sliding Wear Behavior of Sintered and Carburized Steels, Journal of Materials Engineering ad Performance 3(19)(2014)3630-3639

23. K. P. Mingard & B. Roebuck, Mapping complex microstructures in powder metallurgy steels, Powd. Metall. 2010, 53(3) 191-200

24. T. Marcu Puscas, M. Signorini, A. Molinari, G. Straffelini. Image analysis investigation of the effect of the process variables on the porosity of sintered chromium steels. Materials Characterization 50, 1 (2003), p 1–10.

25. S. Saritas, "Effect of porosity on hardenability of PM steels", The Int. J. Powd. Metall. 38(1)(2002)31-40

26. R.M. German, P. Suri, S.J. Park, Review: Liquid phase sintering, J Mater Sci 44(2009)1–39